Arrangement of Apolipoprotein A-I in Reconstituted High-Density Lipoprotein Disks: An Alternative Model Based on Fluorescence Resonance Energy Transfer Experiments†

M. Alejandra Tricerri,‡ Andrea K. Behling Agree,‡ Susana A. Sanchez,§ Jared Bronski,|| and Ana Jonas*,‡

Department of Biochemistry, Laboratory for Fluorescence Dynamics, and Department of Mathematics, University of Illinois at Urbana−Champaign, Urbana, Illinois 61801

Received December 12, 2000; Revised Manuscript Received February 9, 2001

ABSTRACT: The folding and organization of apolipoprotein A-I (apoA-I) in discoidal, high-density lipoprotein (HDL) complexes with phospholipids are not yet completely resolved. For about 20 years, it was generally accepted that the amphipathic helices of apoA-I lie parallel to the acyl chains of the phospholipids ("picket fence" model). However, based on the X-ray crystal structure of a large, lipid-free fragment of apoA-I, a "belt model" was recently proposed. In this model, the helices of two antiparallel apoA-I molecules are extended in a circular arrangement and lie perpendicular to the phospholipid acyl chains. To obtain conclusive information on the spatial organization of apoA-I in discoidal HDL, we engineered three separate cysteine mutants of apoA-I (D9C, A124C, A232C) for specific labeling with the fluorescence probes ALEXA-488 or ALEXA-546 (fluorescein and rhodamine derivatives). The labeled apoA-I was reconstituted into well-defined HDL complexes containing two molecules of protein and dipalmitoylphosphatidylcholine, and the complexes were used in three quantitative fluorescence resonance energy transfer (FRET) experiments to determine the distances between two specific sites in an HDL particle. Comparison of the distances measured by FRET (4.7−7.8 nm) with those predicted from the existing models indicated that neither the picket fence nor the belt model can account for the experimental results; rather, a hairpin folding of each apoA-I monomer with most helices perpendicular to the phospholipid acyl chains and a random head-to-tail and head-to-head arrangement of the two apoA-I molecules in the HDL particles are strongly suggested by the distance and lifetime data.

Apolipoprotein A-I (apoA-I)[1] is the major protein component of high-density lipoproteins (HDL)—it determines the structure and functions of this lipoprotein class. The well-known antiatherogenic properties of HDL (*1*) can be attributed, in part, to their ability to remove cholesterol from peripheral tissues for transport to liver and steroidogenic tissues for metabolism and excretion (*2*). Various steps of this reverse cholesterol transport process depend on the functions of apoA-I: apoA-I binds to cellular receptors (*3*) and transporters (*4*) and solubilizes membrane phospholipids and cholesterol (*5*); in plasma, apoA-I activates lecithin cholesterol acyltransferase (LCAT), resulting in cholesterol esterification on HDL (*6*); also, apoA-I modulates lipid transfers between lipoproteins as well as HDL rearrangements due to the actions of lecithin cholesterol acyltransferase (LCAT), cholesterol ester transfer protein, and phospholipid transfer protein (*7*); finally, apoA-I mediates the delivery of HDL cholesterol esters to steroidogenic tissues and liver (*8*).

The diverse functions of apoA-I depend on its unique structural properties, particularly in the lipid-bound state. The primary sequence of apoA-I contains homologous repeating 11 and 22 amino acid sequences that are known to form amphipathic, lipid-binding helices (*9*). These amphipathic helices, together with phospholipids and unesterified cholesterol, form the outer shell of HDL, surrounding a neutral lipid core in spherical mature particles. In nascent HDL, the lipid core is minimal, so that the phospholipids and cholesterol form a bilayer disk stabilized at the edge by a ring of apoA-I helices. All the amphipathic helices of apoA-I (about

† This work was supported by NIH Grant HL-16059 to A.J. and by a predoctoral fellowship from the American Heart Association, Illinois Affiliate, to A.K.B.A. The spectroscopic experiments were performed at the Laboratory for Fluorescence Dynamics, supported by NIH Center Grant RR-03155.

* To whom correspondence should be addressed at the Department of Biochemistry, College of Medicine at Urbana−Champaign, University of Illinois at Urbana−Champaign, 506 S. Mathews Ave., Urbana, IL 61801. Telephone: (217) 333-0452, FAX: (217) 333-8868, E-mail: a-jonas@uiuc.edu.

‡ Department of Biochemistry.

§ Laboratory for Fluorescence Dynamics.

|| Department of Mathematics.

[1] Abbreviations: apoA-I, apolipoprotein A-I; HDL, high-density lipoprotein; D9C, A124C, and A232C, mutant forms of recombinant proapoA-I containing Cys residues at positions 9, 124, and 232 of the apoA-I sequence; D9C-F (or -R), A124C-F (or -R), and A232C-F (or -R), mutants covalently and specifically labeled with ALEXA-488 (F) or ALEXA-546 (R) Cys-specific fluorescence probes; DPPC, dipalmitoylphosphatidylcholine; DMPC, dimyristoylphosphatidylcholine; POPC, palmitoyloleoylphosphatidylcholine; TBS, 10 mM Tris, 150 mM NaCl, 1 mM NaN_3, 0.01% EDTA, pH 8.0, buffer; PMSF, phenylmethylsulfonyl fluoride; GndHC1, guanidine hydrochloride; DTT, dithiothreitol; TCEP, tris(2-carboxyethyl)phosphine hydrochloride; rHDL, reconstituted HDL; τ, fluorescence lifetime; WMF, wavelength of maximum fluorescence; WT, WT-proapoA-I, wild-type recombinant apoA-I containing a six amino acid pro segment; FRET, fluorescence resonance energy transfer; LCAT, lecithin cholesterol acyltransferase.

10.1021/bi002815q CCC: $20.00
Published on Web 03/29/2001

80% of the sequence) can potentially bind to lipids, but the first and last helices appear to have the highest affinity (*10*). It has been proposed that some of the central helices may bind reversibly to lipids depending on the lipid content and size of the HDL particles (*11*).

Aside from the lipid-binding properties of the amphipathic helices of apoA-I, the fifth helix (repeat 6) of apoA-I (residues 143−165) (*12, 13*) and specific residues within this sequence (Val156 and Arg160) (*14, 15*) are involved in LCAT activation; and central and C-terminal helical regions of the sequence have been implicated in interactions with cells (*8, 16*).

To better understand the diverse functions of apoA-I and its remarkable conformational adaptations, it is essential to determine the three-dimensional organization of apoA-I in at least one lipid-bound form. The simplest, and best characterized HDL are reconstituted HDL (rHDL) particles containing two molecules of apoA-I and a pure phospholipid, such as dimyristoylphosphatidylcholine (DMPC), dipalmitoylphosphatidylcholine (DPPC), or palmitoyloleoylphosphatidylcholine (POPC), in a well-defined discoidal particle. So far, no X-ray structures of these particles are available, but two computer molecular models have been proposed for a large fragment of apoA-I (lacking 43 or 47 N-terminal residues that are thought to adopt a globular structure) on a POPC disk. In the first model, known as the "picket fence" model (*17, 18*), the amphipathic helices of an apoA-I monomer are antiparallel and are joined to each other by sharp turns. The axes of the helices are roughly parallel to the acyl chains of the phospholipids. Relative to each other, the two apoA-I monomers can be arranged head-to-tail or head-to-head (*18*), on the periphery of the rHDL disk. In the second, more recent model known as the "belt model", the apoA-I monomers are extended and almost circular with the second monomer antiparallel and overlapping at the C-terminal end to form a belt of two apoA-I molecules, whose helix axes are perpendicular to the phospholipid acyl chains (*19*).

The objective of this work was to obtain definitive experimental evidence so that a distinction could be made between the two models of apoA-I organization in rHDL particles or to provide the basis for alternative models. Our approach was to use fluorescence resonance energy transfer (FRET) to determine distances between two specific sites of apoA-I reconstituted into rHDL. To specifically label apoA-I with a fluorescence donor or acceptor, we introduced Cys residues into the sequence. While this work was in progress, Li, Sorci-Thomas, and colleagues (*20*) published a similar study and concluded that their results were consistent with the belt model of rHDL. In contrast to their approach, our study uses three different mutants of apoA-I and three quantitative FRET techniques to obtain well-defined distances between at least two sites in apoA-I and to arrive at the conclusion that neither the picket fence nor the belt model represent the organization of apoA-I molecules on rHDL. Rather, we propose head-to-head and head-to-tail hairpin folding of apoA-I, not only to explain the current results but also to explain previous data on the properties of rHDL particles.

MATERIALS AND METHODS

Materials

Dipalmitoylphosphatidylcholine (DPPC), phenylmethylsulfonyl fluoride (PMSF), and sodium cholate were purchased from Sigma Chemical Co.; ultrapure guanidine hydrochloride (GndHCl) and dithiothreitol (DTT) were obtained from Boehringer Mannheim; ALEXA Fluor 488 C_5 maleimide [ALEXA-488, a fluorescein derivative (F)], ALEXA Fluor 546 C_5 maleimide [ALEXA-546, a rhodamine derivative (R)], and tris(2-carboxyethyl)phosphine hydrochloride (TCEP) were purchased from Molecular Probes. Kanamycin sulfate and IPTG were obtained from CalBiochem.

Methods

Site-Directed Mutagenesis. Human proapoA-I cDNA was subcloned into the vector pBluescript KS (Stratagene) and used as a template for the construction of the three single point mutants of proapoA-I (D9C, A124C, A232C). The mutants were constructed using the Quickchange method (Stratagene). The sequences for the coding strands of the mismatch primers were the following (mismatch codons are underlined): D9C, 5N-CCC TGG TGC CGA GTG AAG GAC CTG GCC ACT GTG TAC-3N; A124C, 5N-TAC CGC CAG AAG GTG GAG CCG CTG CGC TGT GAG CTC CAA GAG GGC GCG CGC CAG AAG-3N; A232C, 5N-AAG GTC AGC TTC CTG AGC TGT CTC GAG GAG TAC ACT AAG-3N. The mutations were confirmed by DNA sequencing at the Biotechnology Center (University of Illinois, Urbana−Champaign).

Overexpression and Purification. The mutants and the WT proapoA-I cDNAs were subcloned into the pET-30a expression plasmid, directly downstream of a histidine tag sequence, and transformed into BL-21(DE3) *E. coli* cells (Novagen). An overnight culture was used to inoculate multiple 250 mL Luria−Bertani (LB) cultures supplemented with 30 μg/mL kanamycin. Cells were grown at 37 °C to an $A_{600\ nm}$ of 0.5−0.6, and protein synthesis was induced by incubation with 0.8 mM IPTG for 2 h. Cells were harvested and stored overnight at −80 °C. The pellet was resuspended in buffer containing 0.1 M potassium phosphate, 0.15 M NaCl, 0.1 mM PMSF, 0.1 mM sodium *m*-bisulfite, and 6.5 mM DTT, pH 7.8. The cells were lysed by sonication and spun at 18000*g* for 15 min. The soluble cell contents and the protein obtained from the inclusion bodies, after solubilization with 6 M GndHCl, were applied to a His-binding column (Boehringer-Mannheim), and eluted according to manufacturer's instructions. His-tagged proteins were dialyzed into 10 mM Tris, 150 mM NaCl, 1 mM NaN_3, and 0.01% EDTA, pH 8.0 (TSB), prior to reconstitution into rHDL (see below). The His tag was removed by digesting the rHDL particles with enterokinase (Boehringer-Mannheim) (0.25 μg/mg of protein), at room temperature for 12 h. A second run through the His-binding column yielded WT and proapoA-I variants that were >95% pure (Figure 1A). The lipid-bound proteins in rHDL were dialyzed against 5 mM ammonium bicarbonate and lyophilized. Lipids were extracted with cold ethanol/diethyl ether (3:2) and hexane/2-propanol (3:2).

Labeling of the Mutants with Fluorescence Probes. As it is well-known that the structural and functional properties of plasma apoA-I and recombinant proapoA-I are identical

in vitro (*21*), no distinction will be made between these forms of apoA-I in the remainder of this article. Mutants of apoA-I (typically 1−2 mg) in degassed TSB at pH 7.1 were incubated with the sulfhydryl-specific probes for 1 h at room temperature in the presence of 0.4 mM TCEP. The probes (dissolved in the same buffer) were added in small volumes while stirring in the dark. ALEXA-488 was added to a final molar ratio of 30:1, probe to protein. A molar excess of 5:1, probe to protein, and 0.1% sodium cholate were used for the specific labeling with ALEXA-546. Labeled proteins were separated from unbound probe by elution through PD-10 columns (Pharmacia) and dialysis overnight into TSB buffer for further purification. ApoA-I was reacted alongside the mutants to detect nonspecific labeling. The efficiency of labeling was determined from the molar extinction coefficients [for ALEXA-488, $\epsilon_{492} = 67\,100\ \text{cm}^{-1}\ \text{M}^{-1}$, and for ALEXA-546, $\epsilon_{554} = 90\,300\ \text{cm}^{-1}\ \text{M}^{-1}$ (Molecular Probes specifications); and $\epsilon_{280} = 37\,500\ \text{cm}^{-1}\ \text{M}^{-1}$ for proapoA-I variants]. All three mutants were labeled specifically (molar ratio 0.9 to 1.1 probe to protein). The nonspecific labeling detected with apoA-I was <10%.

Preparation of rHDL Particles. Reconstituted discoidal HDL particles (rHDL) were prepared by the sodium cholate dialysis method (*22*, *23*). A starting DPPC:protein:sodium cholate molar ratio of 100:1:150 was selected in order to obtain relatively pure rHDL, 96 Å in diameter, containing two apoA-I per complex (*24*, *25*). Labeled or unlabeled apoA-I variants (1−2 mg) were used for different experiments. Protein concentration was determined by a modified Lowry method (*26*). The desired amount of DPPC in $CHCl_3$ was dried under N_2. Lipids were dispersed in TSB, and sodium cholate was added and incubated at 50 °C until the preparation was completely clear. Proteins were then added and incubated with the mixed micelles at room temperature for 1 h. The mixture was dialyzed extensively in the dark at 4 °C against TSB. To isolate homogeneous 96 Å rHDL particles and remove traces of free fluorescence probes, all preparations were passed through a Superdex 200 HR 10/30 column (Pharmacia FPLC System) equilibrated with TSB. The homogeneity of the rHDL particles and their diameters were confirmed by native 8−25% PAGGE (Pharmacia Phast System).

Far-UV Circular Dichroism Measurements. Average α-helical contents, as well as free energies of unfolding of the labeled mutants in solution, were measured in order to determine whether the labeling had perturbed the protein structure. Spectra between 250 and 200 nm were recorded at room temperature on a Jasco-720 spectropolarimeter equipped with a PFD-3505 titrator. Proteins at an initial concentration of 0.1 mg/mL in 0.1 M phosphate buffer, pH 8.0, were titrated with a stock solution of GndHCl to a final concentration of 4 M GndHCl, allowing 10 min for equilibration between each addition. The percent of α-helix content of the proteins was calculated from the minimum value of ellipticity at 222 nm (*27*). The free energies of unfolding were calculated from the dependence of the ellipticity values on the concentration of GndHCl (*28*, *29*).

Fluorescence Resonance Energy Transfer (FRET) Measurements. Fluorescence resonance energy transfer is a distance-dependent interaction between the electronic excited states of two fluorescent molecules, in which excitation is transferred from a donor molecule (D) to an acceptor molecule (A), without emission of a photon. The efficiency of energy transfer (E) is related to R_0, the Förster radius, and R, the distance between donor and acceptor, by the equation:

$$E = R_0^6/(R_0^6 + R^6) \tag{1}$$

R_0 represents the distance where the transfer is 50% efficient and is calculated (in centimeters) as follows (*30*, *31*):

$$R_0^6 = (8.79 \times 10^{-25})[n^{-4}Qk^2J(\lambda)] \tag{2}$$

In eq 2, n is the refractive index (taken as 1.4), Q is the quantum yield of the donor in the absence of acceptor, and k^2 is the orientation factor (assumed to be 2/3 for randomly oriented, mobile D and A). $J(\lambda)$, the overlap integral between donor emission and acceptor absorption, is calculated from the spectral data by

$$J(\lambda) = \int_0^\infty [\epsilon_A(\lambda)\cdot\lambda^4] f_D(\lambda)\, d\lambda \tag{3}$$

where $\epsilon_A(\lambda)$ is in $\text{cm}^{-1}\ \text{M}^{-1}$ units and f_D is the fluorescence intensity of the donor at wavelength λ

$$\int_0^\infty f_D(\lambda)\, d\lambda = 1 \tag{4}$$

Homo-FRET Measurements. Fluorophores which exhibit small Stokes shifts, such as fluorescein (or its ALEXA-488 derivative), can effectively undergo self-transfer which can be detected by the resulting depolarization of the emission (*32*). The efficiency of energy transfer can be calculated from the measurement of the polarization (or anisotropy) in the absence and the presence of energy transfer. The expression for the efficiency of energy transfer (E) in terms of anisotropy (r) is (*33*)

$$E = 2(r_0 - \langle r\rangle)/r_0 \tag{5}$$

where r_0 and $\langle r\rangle$ are the observed anisotropies in the absence and presence of energy transfer, respectively. In this study, the ALEXA-488 (F) probe was chosen for the homo-FRET measurements.

For each apoA-I mutant tested, two different preparations of rHDL were necessary: (a) rHDL having all the protein molecules labeled (to measure $\langle r\rangle$); and (b) rHDL in which the labeled variants represented only 10% of the total protein content [to determine anisotropy in the absence of homotransfer (r_0)]. A third preparation, having only unlabeled apoA-I, was reconstituted and used as a control. Steady-state anisotropy measurements were carried out using an ISS PC1 photon counting spectrofluorometer. ALEXA-488 adducts with the apoA-I mutants were excited at 475 nm, and emission was recorded through long-pass filters, OG 550 and HOYA 58. Two slits of 0.1 nm in the excitation beam and two slits of 0.5 nm in the emission beam were used in order to eliminate scattered light. Protein concentrations ranged from 0.01 to 0.075 mg/mL. The rHDL in TBS were diluted into 90% glycerol, and were measured at −3 °C to minimize depolarization due to rotational diffusion. Previous controls showed that the incubation of rHDL with glycerol at −3 °C during the time necessary for the experiment (∼15 min) does not alter particle size and mobility on native PAGGE.

Background due to sample scatter was corrected with control rHDL reconstituted with plasma apoA-I at the same concentration as the labeled samples.

Hetero-FRET Measurements. When the donor and acceptor probes in FRET experiments are chemically different, FRET can be detected by: (a) the increase of the fluorescence intensity of the acceptor; (b) the decrease of the fluorescence intensity of the donor; or (c) the decrease in the fluorescence lifetime of the donor (*31*). For these experiments, ALEXA-488 (F) and ALEXA-546 (R) were chosen as donor and acceptor, respectively; and methods (a) and (c) were selected for the determination of FRET efficiencies and *R* values. For each apoA-I mutant tested, three preparations of rHDL were made differing in the contents of the labeled variants (F and R) and unlabeled apoA-I: (a) F/apoA-I (molar ratio, 1:1); (b) F/R (molar ratio, 1:1); and (c) apoA-I/R (molar ratio, 1:1).

(a) Determination of the Enhancement of the Acceptor Fluorescence Emission. Efficiency of FRET (*E*) was calculated from spectral data as described by Gohlke et al. (*34*). This approach allows the calculation of *E* from three fluorescence spectra and corrects for the concentration of labeled apoA-I and for errors in the percentage of acceptor labeling. The fluorescence emission spectrum of rHDL containing F/R, $F(460, \lambda_{em})$ (excited at 460 nm), is fitted to the weighted sum of two spectral components: (a) a standard emission spectrum of an rHDL labeled only with donor, $F^D(460, \lambda_{em})$, and (b) a spectrum of the rHDL containing F/R, $F(530, \lambda_{em})$ (excited at 530 nm where only the acceptor absorbs):

$$F(460, \lambda_{em}) = [a \cdot F^D(460, \lambda_{em})] + [(\text{ratio})_A \cdot F(530, \lambda_{em})] \quad (6)$$

The coefficients a and $(\text{ratio})_A$ are the fitted fractional contributions of the two spectral components; $(\text{ratio})_A$ is the acceptor fluorescence signal due to FRET from the donor, normalized by $F(530, \lambda_{em})$ as given by Gohlke et al. (*34*):

$$(\text{ratio})_A = \{F(460, \lambda_{em}) - [a \cdot F^D(460, \lambda_{em})]\}/F(530, \lambda_{em})$$

$$(\text{ratio})_A = \{E[\epsilon^D(460)/\epsilon^A(530)] + \epsilon^A(460)/\epsilon^A(530)\} \quad (7)$$

In eq 7, ϵ^D and ϵ^A are the molar absorption coefficients of F(D) and R(A) at the given wavelengths, respectively; $\epsilon^D(460)/\epsilon^A(530)$ and $\epsilon^A(460)/\epsilon^A(530)$ were determined from the excitation spectra of D and A in singly labeled rHDL preparations (F/apoA-I and apoA-I/R). Since labeled apoA-I exists as "dimers" in rHDL (rHDLs have two molecules of apoA-I), the possible species that are present in the F/R rHDL preparation are DD, AA, and AD. Because 1:1 molar ratios of D/A were used in the F/R rHDL preparation, the probability of DD and AA is 25% and of AD is 50%. The rHDL species containing AA or DD would be twice as fluorescent as an rHDL containing only one acceptor- or donor-labeled monomer. With this consideration in mind, in the calculation of $(\text{ratio})_A$, we assumed the direct emission of the acceptor (excited at 460 or 530 nm) to be double of the experimental values.

Steady-state fluorescence spectra were recorded at room temperature on the same equipment used for fluorescence anisotropy, but measurements were performed under magic angle conditions. ALEXA-488 was excited at 460 nm, and the emission was recorded between 470 and 600 nm. Direct excitation of ALEXA-546 was achieved at 530 nm, and the emission was recorded between 540 and 600 nm. Protein concentrations were 0.04 mg/mL in all the experiments.

(b) Measurement of the Decrease in the Fluorescence Lifetimes of the Donor. Efficiency (*E*) of FRET is related to the lifetime of the donor by (*30*)

$$E = 1 - (\tau_{da}/\tau_d) \quad (8)$$

where τ_{da} and τ_d are the fluorescence lifetimes of the donor in the presence and in the absence of acceptor, respectively.

Fluorescence lifetimes of ALEXA-488 were measured using the multifrequency phase and modulation method. Excitation was achieved using the 488 nm line of an argon ion laser, passed through a 488 nm band-pass filter to avoid scattered light. Emission was detected through OG 550 and Corion 520 P10 long-pass filters using magic angle conditions. Fluorescein (lifetime 4.0 ns) was used as a lifetime reference. Phase and modulation data were collected at 20 °C across a harmonic range of 10−200 MHz. Analyses were performed using the GLOBAL Unlimited software with a constant error of 0.2° for the phase and 0.004 for the modulation. A model of two discrete lifetime components was used, and the goodness of fit was judged by the value of the reduced chi-square (χ^2).

To account for the presence of rHDL containing two donors, a correction is applied. For a random distribution of D and A in a 1:1 mixture, 25% of the rHDL would contain two molecules of D, implying that the lifetime of 50% of the donor molecules is not affected by FRET, but rather has the same value as that measured in the absence of A $\langle\tau_d\rangle$. Homotransfer between D molecules does not affect lifetimes. The corrected average lifetime $\langle\tau_c\rangle$ was obtained from the measured value $\langle\tau_{da}\rangle$ by

$$\langle\tau_{da}\rangle = 0.5\langle\tau_c\rangle + 0.5\langle\tau_d\rangle \quad (9)$$

Contribution of the Probe Dimensions to the Effective Distance in Molecular Models of rHDL. Dimensions of the probes, from the Cys attachment site to the center of the aromatic rings, were estimated at 1.5 nm (Weblab Software). Movements of the probes were taken into account due to the flexibility of the linker chain connecting the fluorescent ring to the protein in estimating the efficiency of FRET (*E*) and *R* predicted from the molecular models of rHDL. The average contribution of the probes to the distance (*R*) was estimated by a Monte Carlo simulation, considering a local rotation of the probe around the covalent link (θ_1, θ_2), and a movement of the molecule in the plane of the rHDL (ϕ_1, ϕ_2). The *E* averaged over 100 000 points $\langle E\rangle$ was estimated as follows:

$$\langle E\rangle = \langle R_0^6/(R_0^6 + R^6)\rangle = R_6^0 \sin[\theta_1] \sin[\theta_2]/$$
$$\{[(a \sin[\theta_1] \cos[\phi_1] - a \sin[\theta_2] \cos[\phi_2] + b)^2 +$$
$$(a \sin[\theta_1] \sin[\phi_1] - a \sin[\theta_2] \sin[\phi_2])^2 +$$
$$(a \cos[\theta_1] - a \cos[\theta_2])^2]^3 + R_0^6\} \quad (10)$$

where R_0 is the Förster radius (taken as 5.0 nm) and *R* is the variable distance between the Cys residues in rHDL; *a* is

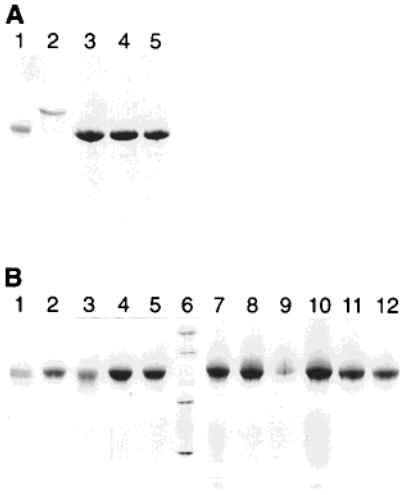

FIGURE 1: Panel A: SDS−PAGE showing the high purity (>95%) of the recombinant proapoA-I Cys mutants. Lane 1, plasma apoA-I; lane 2, D9C mutant prior to removal of the his-tag; lane 3, D9C proapoA-I mutant; lane 4, A124C mutant; lane 5, A232C mutant. Panel B: Native polyacrylamide gradient gels (8−25%) of rHDL containing POPC/proapo mutants with ALEXA-488 (F) and/or ALEXA-546 (R) probes made with initial POPC:protein molar ratios of 100:1 and purified as described under Materials and Methods. Lanes from 1 to 11 represent various combinations of labeled and unlabeled apoA-I rHDL; lane 6 contains protein size markers; and lane 12 represents a control rHDL with unlabeled apoA-I.

the dimension of the probe (1.5 nm), and *b* is the distance between the Cys residues estimated from the coordinates of the molecular models (*18, 19*).

RESULTS

Properties of the ApoA-I Variants Labeled with Fluorescence Probes. ApoA-I and proapoA-I do not contain Cys residues in their sequences; therefore, Cys residues were introduced into specific positions (D9C, A124C, A232C) as sites for subsequent labeling with Cys-specific fluorescence probes suitable for FRET measurements. The expression and purification procedures used in this study gave high yields of pure proteins (Figure 1A). The apoA-I mutants were then labeled specifically and stoichiometrically (1 probe per protein) with ALEXA-488 (F), as the donor, and ALEXA-546 (R), as the acceptor probes. These probes were selected because their fluorescence properties are very similar to those of fluorescein and rhodamine, respectively, a well-known and thoroughly tested pair of fluorescence probes in FRET measurements (*20, 31, 34*). Furthermore, the ALEXA probes are water soluble, which facilitates specific and stoichiometric labeling of the individual Cys residues in the apoA-I mutants. The positions for the introduction of the Cys residues were selected to be in the N-terminus (D9C), C-terminus (A232C), and center of the apoA-I sequence. From the molecular models of rHDL (*18, 19*), the A124C and A232C positions are in distinct locations in the circumference of the rHDL (see Figure 5) and should be easily distinguished experimentally. The D9C position, although not modeled by computer, can serve as an additional point of reference in examining the validity of existing models and in predicting the location of the globular N-terminal region of apoA-I relative to the rest of the molecule.

Prior to the FRET experiments, the fluorescent-labeled apoA-I mutants were characterized for their structural properties and stability to denaturation in the lipid-free state. As shown in Table 1, the WMF of the Trp residues are comparable for all the labeled proteins, suggesting that the average environment of the Trp residues and the three-dimensional structure in the N-terminal half of the molecules are similar to the control apoA-I. The contents of α-helix are also comparable, although the ALEXA-546 (R) conjugates may have a slightly decreased α-helix content compared to the apoA-I control. The free energies of unfolding are similar (within experimental error) for all the apoA-I forms.

Table 1: Spectral Properties and Stabilities of Lipid-Free ApoA-I Cysteine Mutants Labeled with ALEXA-488 (F) or ALEXA-546 (R) Probes

protein	WMF Trp[a] (nm)	α-helix[b] (%)	$\Delta G°$ denat[c] (kcal/mol)
apoA-I	334 ± 2	57 ± 7	2.5 ± 0.3
D9C-F	ND	56	2.5
A124C-F	336	59	2.8
A232C-F	336	53	3.0
D9C-R	336	48	2.2
A124C-R	335	46	2.2
A232C-R	ND	49	ND

[a] Wavelength of maximum fluorescence (WMF) is the average for the 5 Trp residues in the mutant forms of proapoA-I, or the average of 4 Trp for plasma apoA-I. [b] The α-helix content was calculated from CD measurements at 222 nm using the expression of Chen et al. (*27*). Protein concentrations were determined by the Markwell et al. method (*26*). [c] Free energy of denaturation determined from CD molar ellipticity values, measured at equilibrium as a function of GndHCl concentrations, and fitted to the equation for $\Delta G°$ of denaturation (*28, 29*).

Previous experiments with Cys mutants of apoA-I, labeled with the acrylodan probe (*35*), showed that small differences in the structure of the lipid-free proteins are minimized in the lipid-bound rHDL state. In fact, all the apoA-I variants in this study formed rHDL complexes with high efficiency and identical 96 Å (9.6 nm) diameters as shown in Figure 1B. Thus, it is safe to assume that the overall conformation of the apoA-I variants is the same as that of control apoA-I in the rHDL particles that were employed in subsequent FRET experiments.

Determination of Distances by Homo-FRET. The R_0 distance measured for ALEXA-488, using eqs 2−4, in rHDL conjugates was 5.0 nm. Under the experimental conditions of low protein concentration, low temperature, and high viscosity, depolarization of fluorescence occurs by energy transfer between ALEXA-488 probes on the same rHDL particle, and depolarization due to rotational diffusion is minimized (*32*). To confirm that energy transfer occurs between probes on the same rHDL particle, rHDL preparations containing 10, 25, 40, and 100% labeled apoA-I were examined. The fluorescence anisotropy decreased with increasing proportion of label, as expected, and confirmed that essentially no energy transfer occurs in the 10% labeled sample.

Table 2 shows the anisotropy values, $\langle r \rangle$ and r_0, obtained for the various labeled variants of apoA-I in rHDL. The r_0 values (0.34) are all similar due to the immobilized probes and the absence of energy transfer. The difference in r_0 for the free ALEXA-488 probe probably reflects the protein and lipid environments of the probe in the rHDL particles, in addition to the 90% glycerol solution. The $\langle r \rangle$ values, in contrast to r_0, vary between 0.24 and 0.31 for the rHDL

Table 2: Fluorescence Anisotropy Parameters for FRET Analysis of Homotransfer between ALEXA-488 (F) Probes Attached to Specific Cys Residues of ApoA-I Mutants (D9C, A124C, A232C) Reconstituted into rHDL Particles, Each Containing 2 ApoA-I Molecules

ALEXA-488 (F) labeling positions	$\langle r \rangle^a$	$r_0{}^b$	E^c	R^c (nm)
9−9	0.311	0.349	0.21	6.2
124−124	0.268	0.346	0.45	5.2
232−232	0.244	0.341	0.56	4.8
9−232	0.283	0.340	0.34	5.6
free ALEXA-488 probe		0.361		

[a] Fluorescence anisotropy measured at −3 °C in 90% glycerol at a 475 nm wavelength of excitation for rHDL containing 100% labeled apoA-I, i.e., 2 probe molecules per rHDL. [b] Fluorescence anisotropy measured under the same conditions as $\langle r \rangle$ but on rHDL particles containing 10% labeled apoA-I and 90% unlabeled apoA-I to minimize homotransfer. [c] *E*, efficiency of FRET; *R*, experimental distance between the probe molecules on an rHDL particle determined using eqs 5 and 1.

samples and reflect the distances between the ALEXA-488 probes. The calculated values of *E* and *R* are listed in Table 2. Similar results were obtained when the anisotropy measurements were performed at ambient temperature and in the absence of glycerol, but rotational motions of the probes resulted in much lower anisotropy values and less accurate data.

Determination of Distances from the Enhancement of Acceptor Fluorescence. The R_0 distance for 50% energy transfer from the ALEXA-488 (F) donor to the ALEXA-546 (R) acceptor in rHDL particles was calculated to be 5.7 nm.

Figure 2 shows a typical set of fluorescence spectra obtained for the rHDL prepared with apoA-I labeled with F (donor) or R (acceptor) at a specific position. Samples of rHDL containing only F or only R were used as controls. When the donor (F) is excited in the double-labeled sample (F/R), a decrease in the intensity of donor (F) emission is observed, accompanied by an increase in the emission of the acceptor (R) due to FRET. Spectra for rHDL samples containing only donor (F) or acceptor (R) were measured under the same conditions. A small contribution to the intensity due to direct excitation of the acceptor (R) at 460 nm is observed, and subtracted in subsequent calculations.

The addition of detergent (0.3% SDS) results in the disappearance of the peak corresponding to the acceptor fluorescence sensitized by FRET. As SDS solubilizes rHDL components in mixed micelles, the separation of apoA-I molecules abolishes the FRET process (Figure 3).

To confirm that FRET occurs between probes within the same rHDL and that there is no energy transfer between probes located in different particles, we measured the spectra of particles containing only donor or only acceptor after exciting at 460 nm (Figure 4A). The arithmetic sum of these spectra is indistinguishable from the spectra obtained for both samples, mixed together (Figure 4B). This is clear evidence that there is no interparticle energy transfer. Table 3 gives the $(\text{ratio})_A$ and the efficiency (*E*) of FRET obtained from the spectral data, and the distances (*R*) calculated from eq 1 for various rHDL samples containing donor (F) and acceptor (R) probes in different positions.

Lifetimes of the ALEXA-488 (F) Donor. Table 4 displays the lifetimes (fractional and average), as well as the fractional

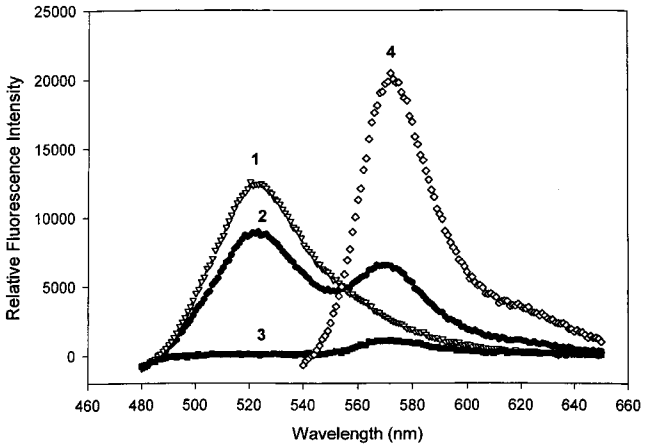

FIGURE 2: Fluorescence emission spectra for rHDL preparations containing the apoA-I ALEXA-488 (F) donor and/or ALEXA-546 (R) acceptor probes. The sample spectra are for apoA-I labeled with F or R at position 232. The spectra correspond to: 1 (▽) F:A-I rHDL excited at 460 nm; 2 (●) F:R rHDL excited at 460 nm; 3 (■) A-I:R rHDL excited at 460 nm; 4 (◇) F:R rHDL excited at 530 nm. All samples contained 0.04 mg/mL protein.

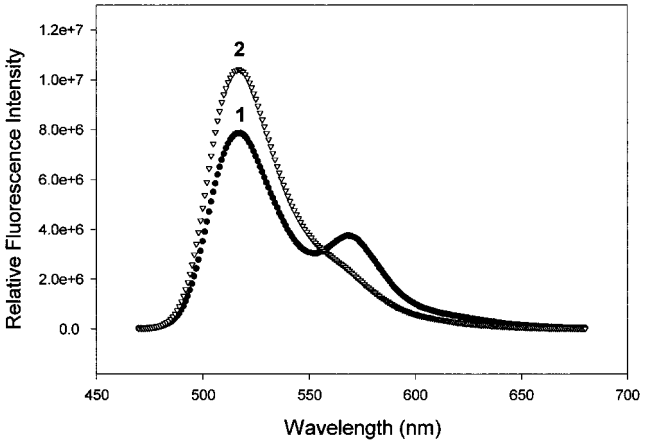

FIGURE 3: Fluorescence emission spectra for an rHDL labeled in position 232-F and position 9-R, excited at 460 nm. Spectrum 1 (●) shows FRET by the emission peak at 570 nm; spectrum 2 (▽) shows the elimination of FRET when 0.3% SDS is added to the rHDL sample. The donor intensity increases at 515 nm, and the acceptor intensity is essentially eliminated at 570 nm.

contribution values (*f*) for ALEXA-488 in the presence and absence of the ALEXA-546 acceptor on the same rHDL particle. Table 4 also shows the efficiency (*E*) of energy transfer calculated from lifetime values using eq 8 and the corresponding distances (*R*) using eq 1.

The major fluorescence lifetime contribution (>90%) for all the ALEXA-488 adducts comes from a species with a lifetime between 3.68 and 4.15 ns; a minor contribution (<10%) comes from a short-lifetime component (0.5−0.92 ns). Rather than a separate probe population, the short lifetime could represent a distinct conformation of the probe. However, for all practical purposes, a single, uniform population of fluorescence donors can be assumed for each rHDL species. For the samples containing both, donor and acceptor, the average lifetimes are decreased as a result of FRET. After a correction is applied (eq 9) to account for the distribution of donor molecules in the rHDL samples containing both probes, $\langle \tau_c \rangle$ values are obtained and are used for the calculation of *E* and *R* values using eq 8 and eq 1.

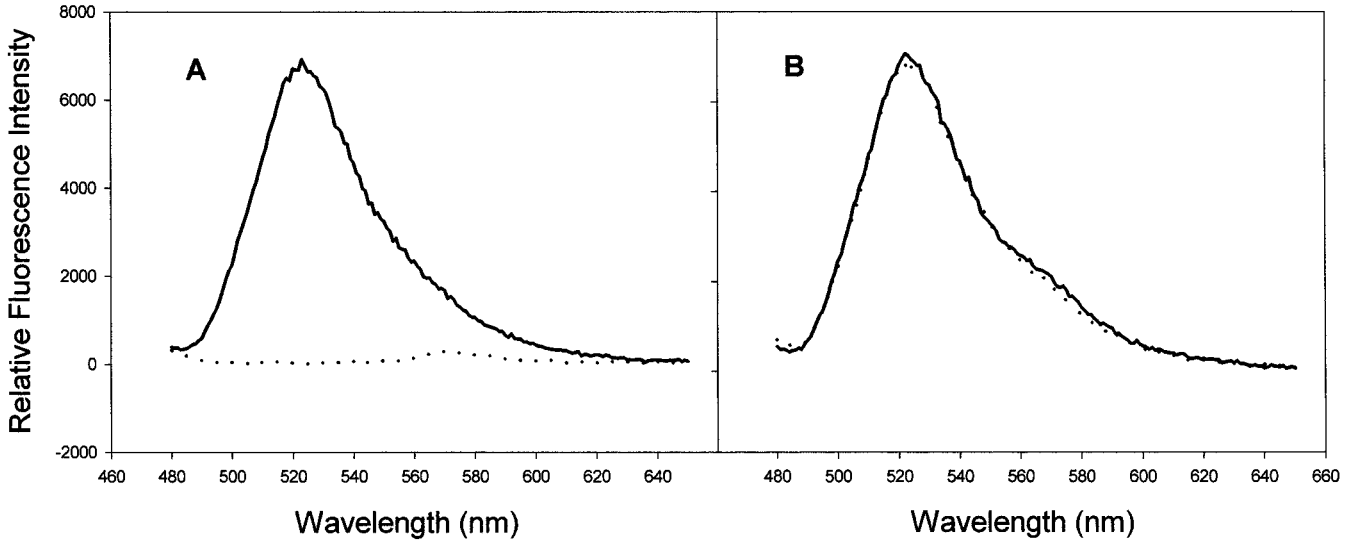

FIGURE 4: Additivity of fluorescence emission spectra for separate rHDL particles labeled with 232-F or 9-R. Panel A shows the spectra of the individual samples excited at 460 nm. Panel B shows the experimental spectrum for a mixture of both rHDLs (—) and, superimposed (···), the sum of the spectra from panel A. The total protein concentration in both panels is 0.04 mg/mL.

Table 3: Measurement of FRET Efficiencies (E) and Distances (R) from the Enhancement of Acceptor (ALEXA-546) Fluorescence When Donor (ALEXA-488) Is Excited in rHDL Particles Containing both Donor and Acceptor Molecules at Specific Sites on ApoA-I

donor (F) and acceptor (R) positions	$(\text{ratio})_A$[a]	E[b]	R[c] (nm)
9(F)−9(R)	0.20	0.35	6.3
124(F)−124(R)	0.36	0.75	4.7
232(F)−232(R)	0.31	0.64	5.3
9(F)−232(R)	0.28	0.53	5.6

[a] The $(\text{ratio})_A$ was obtained from experimental emission spectra using eq 6 as explained under Materials and Methods. [b] E, the efficiency of FRET, was determined from $(\text{ratio})_A$ and the appropriate excitation spectra using eq 7. [c] R, the experimental distances, were calculated using E values and eq 1.

Distances from Computer Models and Corrections for the Dimensions and Flexibility of the Probes. The distances from the computer-generated models of rHDL, between positions 124−124 and 232−232 in the apoA-I sequences, are listed in Table 5 and illustrated in Figure 5. The dimensions and flexibility of the probe (e.g., ALEXA-488) were also considered, because the probe length (1.5 nm) is not negligible compared to the outer diameter of the rHDL, 9.6 nm (*18*), or distances between the Cys α-carbons, obtained from the computer models (1.2−8.3 nm) (*18*, *19*). Table 5 gives the average $\langle E \rangle$ values and average corrected distances R, assuming that the probe moves in a hemisphere with a maximum radius, $a = 1.5$ nm, and is separated from the second probe by the distance (d) determined from the computer models. The orientation of the two hemispheres, swept by the probes, relative to each other was based on the location of the labeled amino acid residue in the corresponding modeled helix and its expected orientation with respect to the protein and lipid in the rHDL.

For example, in the 124−124 situation for the head-to-tail picket fence model (Figure 5A), residue 124 is the first residue in helix 4 (or repeat 5) opposite helix 3 (*18*). Because many of the polar faces of apoA-I helices have a negatively charged central ridge (*9*), it is likely that the negatively charged probes will extend into solution, away from the protein and lipid surface. Both probes are on the same side of the rHDL plane; therefore, a reasonable approximation is that of two hemispheres of radius 1.5 nm on the same plane, separated by a distance d. In the belt model (*19*), residue 124 is in position 4 on the R face of the corresponding helix, pointing toward the solvent and the lipid headgroups. A planar surface of protein and lipid can also be assumed, with the $a = 1.5$ nm hemispheres separated by a distance $d = 2.3$ nm.

In the 232−232 case, in both models, the 232 residue is near the middle of a helical segment, facing toward the lipid. Thus, for both models, the flexible linker of the probe must "snorkel" between protein helices or through lipid to expose the negatively charged fluorescent groups to solvent. In each situation, both a and d are adjusted by about 0.5−1.0 nm.

Regardless of the geometry used to account for the probe length and flexibility, it is evident that the corrected average distances are not greatly affected when d is large compared to a (as in the case of the picket fence model in the head-to-tail configuration). However, the correction can be quite large when d is relatively small as in the case of the belt model.

DISCUSSION

The issue of the orientation of apoA-I helices in rHDL or nascent HDL (parallel or perpendicular to the phospholipid acyl chains) has considerable importance for the elucidation of the mechanism of assembly and functions of these lipoproteins. It is known that after binding to the surface of DMPC vesicles, apoA-I penetrates and lyses the bilayers to give rise to discoidal rHDL (*36*). The orientation of apoA-I on the rHDL products may indicate either a perpendicular insertion of helices into the phospholipid bilayer or a more complex mechanism of apoA-I interaction with an abstraction of membrane phospholipids. Also, the orientation of apoA-I on nascent HDL would affect significantly the possible modes of interaction between apoA-I molecules on the same particle, and with lipid-free apolipoproteins and other plasma proteins. Finally, the orientation of apoA-I on discoidal HDL would affect the nature of the structural rearrangements that

Table 4: Fluorescence Lifetimes of the ALEXA-488 (F) Donor Probe in Specific Sites of ApoA-I Mutants Reconstituted into rHDL Particles (2 ApoA-I Molecules/rHDL). FRET Analysis of Heterotransfer between F and R Probes Based on Donor Lifetime Values

donor (F) and acceptor (R) positions	τ_1,[a] ns (f_1)[a]	τ_2,[a] ns (f_2)[a]	$\langle\tau_{da}\rangle$ and $\langle\tau_d\rangle$[b](ns)	χ^2 [c]	$\langle\tau_c\rangle$[d] (ns)	E[e]	R[f] (nm)
9(F)−9(R)	3.68 (0.93)	0.87 (0.07)	3.48	0.95	3.23	0.13	7.8
9(F)−A-I	3.85 (0.96)	0.79 (0.04)	3.73	0.72			
124(F)−124(R)	3.95 (0.94)	0.71 (0.06)	3.76	1.17	3.45	0.15	7.6
124(F)−A-I	4.10 (0.99)	0.82 (0.01)	4.07	0.10			
232(F)−232(R)	3.99 (0.94)	0.65 (0.06)	3.79	0.97	3.50	0.14	7.7
232(F)−A-I	4.15 (0.98)	0.50 (0.02)	4.08	0.66			
9(F)−232(R)	3.75 (0.92)	0.92 (0.08)	3.52	0.92	3.31	0.11	8.1

[a] Lifetimes (τ_1, τ_2) and fractional contributions (f_1, f_2) from two-exponential analysis of time-resolved phase and modulation measurements. [b] Average lifetimes calculated from $\langle\tau\rangle = \tau_1 f_1 + \tau_2 f_2$; $\langle\tau_d\rangle$, donor alone; $\langle\tau_{da}\rangle$, donor and acceptor present on the rHDL. [c] Reduced chi-square value for the fit of two discrete exponentials assuming errors of 0.2° and 0.004 for the phase and modulation data, respectively. [d] Average lifetimes corrected according to eq 9. [e] Efficiency of FRET calculated from eq 8, using the corrected $\langle\tau_c\rangle$ lifetimes. [f] Distance between probes calculated from eq 1.

Table 5: Distances from Molecular Models of ApoA-I Organization in rHDL Particles and Corrections Due to Probe Dimensions and Motions

model and labeled residue	simulated distance[a] (nm)	$\langle E\rangle$[b]	average corrected distance[b] (nm)
picket fence model			
124−124	8.3	0.063	7.8
232−232[c]	7.8	0.032	8.8
232−232[c]	7.8	0.066	7.8
belt model			
124−124	2.3	0.92	3.4
232−232[c]	1.2	0.96	2.9
232−232[c]	1.2	0.98	2.7

[a] Distances obtained from the coordinates of the published computer molecular models of rHDL particles (*18, 19*). The picket fence model is in the head-to-tail conformation. The distances are between the α-carbons of the residues at positions 124 or 232 in the 2 apoA-I molecules on the same rHDL particle. [b] Calculated average FRET efficiencies, $\langle E\rangle$, and corrected average distances accounting for probe dimensions and motions, as described under Materials and Methods and eq 10. The average corrected distances are calculated from $\langle E\rangle$ and eq 1. [c] For each model, two distinct orientations for the flexible linker of the probe at (232−232) relative to the protein−lipid interface are possible. Both were modeled and used in the average $\langle E\rangle$ and corrected distance calculations.

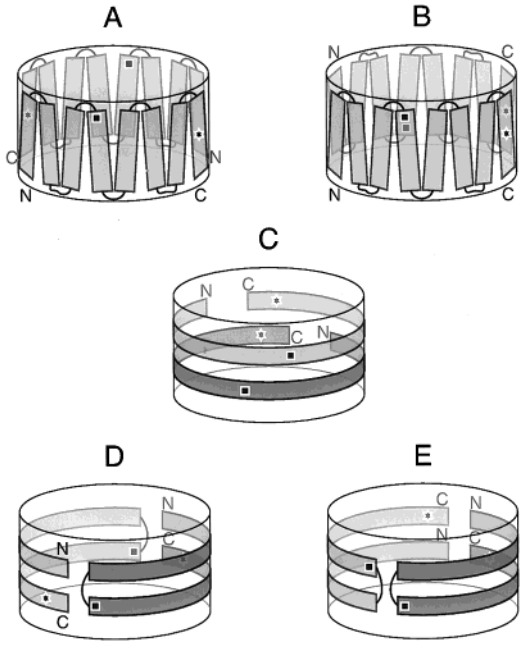

FIGURE 5: Diagrams of rHDL models showing the positions of the labels in the sequences of the two apoA-I molecules. The approximate positions of the Cys residues in the apoA-I mutants are shown for A124C (■) and A232C (closed star in open star); N and C designate the N-terminus and C-terminus of each apoA-I molecule. A: Head-to-tail picket fence model (*18*); the distances between positions 124−124 and 232−232 are given in Table 5. B: Head-to-head picket fence model (*18*); estimated distances between positions 124−124 and 232−232 are 8.0 and 1.5 nm, respectively. C: Belt model (*19*); the distances between positions 124−124 and 232−232 are given in Table 5. D: Proposed hairpin model in the head-to-tail configuration; estimated distances between positions 124−124 and 232−232 are 8.0 and 8.0 nm, respectively. E: Proposed hairpin model in the head-to-head configuration; estimated distances between positions 124−124 and 232−232 are 2.4 and 3.5 nm, respectively.

apoA-I undergoes with changing lipid and protein contents and compositions during metabolism.

Since high-resolution structures of HDL are not yet available, the determination of distances between specific points on apoA-I, in well-defined rHDL particles, can provide valuable information on the overall fold of the protein and its relationship to the other apoA-I molecules on the rHDL and can discriminate between the alternative models of apoA-I orientation in rHDL (*18, 19*). FRET, a well-established method for the determination of distances in macromolecules (*31*−*34*), is especially suitable for these purposes.

Fluorescein and rhodamine is a widely used donor−acceptor pair for FRET measurements. The R_0 distance for this pair of fluorophores is around 5.7 nm, which makes it appropriate for many structural studies in proteins (*20*, *37*) as well as in nucleic acids (*31*, *34*). However, due to the affinity of these fluorophores for the hydrophobic regions of some proteins, in particular apoA-I (unpublished results, Tricerri and Jonas, 1999), specific labeling is difficult to attain. In contrast, the homologues of fluorescein and rhodamine, the ALEXA-488 and ALEXA-546 dyes, respectively, are much more water soluble, due to a high negative charge, resulting in stoichiometric highly specific labeling of apoA-I. In addition, the ALEXA dyes have higher extinction coefficients and quantum yields and are more photostable than the parent compounds.

A recent study by Li, Sorci-Thomas, and colleagues (*20*) used a qualitative FRET approach to help discriminate between the two current models for the orientation of apoA-I in rHDL (*18, 19*). With fluorescein and rhodamine as the donor−acceptor pair, attached to a Cys engineered into position 132 of apoA-I, they observed energy transfer between the two probes when the labeled apoA-I were reconstituted into rHDL disks having 100 Å diameters. These

authors predicted that the separation of the probes in the picket fence model (~10 nm) would be too great to observe energy transfer, whereas the 16 Å separation in the belt model would result in very efficient energy transfer. Even though only a 40% efficiency of transfer was observed, the authors attributed the result to an uneven distribution of the donor and acceptor probes and increased proportion of acceptor−acceptor rHDL, and selected the belt model as the preferred apoA-I orientation. They mentioned an alternative, hairpin conformation, but did not explore further such a model. The experimentally observed efficiency of energy transfer by Li et al. (*20*) of 40% agrees reasonably well with our results for the apoA-I labeled at Cys-124, on the same helix as Cys-132 (Tables 2 and 3), which leads to calculated distances from 4.7 to 5.2 nm between the probes, clearly intermediate between the distances predicted by the two models (Table 5).

In view of the reported rhodamine dimers (*20*), we reexamined the excitation spectra of ALEXA-546 in rHDL and in solution and found a shoulder at 515 nm, that may be analogous to the nonfluorescent dimer feature described by Li et al. (*20*). However, excitation of ALEXA-546 at 530 nm (used in energy transfer measurements) or at 560 nm (near the maximum excitation wavelength) gave fluorescence intensities proportional to the extinction coefficients at 530 and 560 nm, indicating that a single fluorescent species is excited in the 530−560 nm spectral range. Furthermore, examination of literature references (*38*) and Molecular Probes data (*39*) indicated that a shoulder around 515−520 nm occurs in the excitation spectra of monomeric rhodamine dyes, and is very similar to our observation for apoA-I labeled with ALEXA-546 and reconstituted into rHDL particles. Therefore, considering these facts, plus the repulsion expected between negatively charged ALEXA-546 moieties opposing dimer formation, we believe that the putative dimers of rhodamine reported by Li et al. (*20*) are irrelevant for our experimental system.

In this study, we used two quantitative FRET methods to determine experimentally the distances between selected positions of two apoA-I molecules in rHDL complexes (see Figure 5). The distance ranges that can be examined by using ALEXA-488 homotransfer or ALEXA-488 to ALEXA-546 heterotransfer depend on the Förster distances, $R_0 = 5.0$ or 5.7 nm, respectively, and the R^6 dependence of eq 1. Given that experimental errors are around 5%, then E values below 5% or above 95% cannot be discriminated; therefore, the effective range of distances that can be measured by homotransfer is 3.1−8.2 nm, and by heterotransfer is 3.5−9.3 nm.

The method of homotransfer between two ALEXA-488 probes is the simplest, and has the great advantage that fluorescence anisotropy values are independent of the concentration of fluorescent molecules (*32*). Furthermore, homotransfer does not result in lifetime or fluorescence intensity changes because the spectral properties of the donor and acceptor species are identical. The results shown in Table 2 indicate measurable efficiencies of energy transfer and distances between 4.8 and 6.2 nm between the various labeled pairs.

Another complementary FRET method is based on the enhancement of acceptor fluorescence (*31, 34*). This approach has the advantage that the acceptor fluorescence, sensitized by energy transfer, is normalized by the acceptor fluorescence excited where the donor does not absorb (530 nm), thus removing protein concentration effects, quantum yield of the acceptor, and even incomplete labeling by the acceptor probe, as factors affecting fluorescence intensity. This method gives the results shown in Table 3. Compared to the results of Table 2, the agreement is quite good, lending strong support to the validity of the distance measurements by both FRET methods.

The lifetimes of the donor were measured in the absence and presence of acceptor in the rHDL (see Table 4). The decrease in the donor lifetimes in the presence of acceptor and the calculated efficiencies were much less than expected from the FRET results shown in Tables 2 and 3. A similar observation was also made by Li et al. (*20*), and may be explained by the presence of two populations of donor−acceptor pairs: one in which the donors and acceptors are very close so that the extremely short lifetimes are not measurable and do not contribute to the average lifetime (*31*); and another population, where the donor−acceptor pairs are far enough apart so that the lifetime change is small compared to the lifetime of donor alone, and gives R's of approximately 7.7 nm. Also, the fact that a single population of ALEXA-488 probes is observed (92−98% fractional contribution) attests to the complete and specific labeling of apoA-I with this probe, and most likely with the ALEXA-546 probe as well.

Our conclusion from the FRET measurements is that neither the picket fence nor the belt model of apoA-I in rHDL is supported by our results; rather, both models are excluded. A possible alternative is a hairpin configuration of apoA-I in an approximately equal distribution between a head-to-tail and head-to-head arrangement of the two apoA-I molecules (Figure 5, D and E). Since fluorescence intensities and anisotropies are additive, half of the particle population undergoing FRET with very high efficiency (for distances less than 3.0 nm) and the other half undergoing little or no FRET (for distances around 8.0 nm) would give intermediate E and R values. For the case of donor fluorescence lifetimes, very high efficiency of transfer eliminates the contribution from the very short distances, and leaves an apparently homogeneous population with only slightly decreased lifetimes corresponding to distances around 7.7 nm. Thus, the hairpin models (in about 50:50 proportion), shown in Figure 5, do fulfill the requirements for the observed FRET results.

A hairpin arrangement of the apoA-I in rHDL has been suggested previously by Rogers et al. (*40*). Support for such a model comes from a number of experimental sources. There is mounting evidence that some, if not all, of the α-helices of apoA-I in discoidal rHDL are arranged perpendicular to the phospholipid acyl chains (*41, 42*). Also, in these particles, the Trp residues (Trp-50, Trp-72, Trp-108) are far apart from each other, so that the energy transfer effects seen in the helix bundle arrangement of the lipid-free apoA-I are eliminated, suggesting that helices 1, 2, and 3 of apoA-I are extended in rHDL rather than antiparallel to each other (*43*) as predicted by the picket fence model.

Discoidal rHDL particles can be prepared to contain two, three, or four apoA-I molecules on the edge of each disk (*24, 44*). The hairpin model, but not the belt model, can account readily for the existence of all these particles. Furthermore, apoA-I in rHDL is known to undergo structural

rearrangements in the central region of the molecule upon loss of phospholipids (*14*, *24*, *45*) or binding of apoA-II (*25*). Such structural changes can be envisioned to occur in the hairpin arrangement of apoA-I, but are difficult to explain in the belt model constrained by extensive salt bridges and a precise register of the two apoA-I molecules. However, if the apoA-I molecules were allowed to slide relative to each other (*46*), then the belt model would be more versatile in explaining some, but not all, of the experimental observations.

Although more experiments are needed to define precisely the folding and the arrangement of the apoA-I molecules of apoA-I on the periphery of rHDL disks, the present results discount the picket fence (*18*) and original belt (*19*) models, and strongly suggest a hairpin arrangement of apoA-I in these HDL complexes.

ACKNOWLEDGMENT

We are deeply indebted to Dr. T. Hazlett of the Laboratory for Fluorescence Dynamics, University of Illinois at Urbana−Champaign, for his help and advice in using the fluorescence instrumentation. Drs. B. Clegg, C. Gohlke, and O. Holub of the Physics Department, University of Illinois at Urbana−Champaign, were particularly helpful in discussions of FRET theory, measurements, and interpretation of results. Mr. J. Phillips of the Beckman Institute, University of Illinois at Urbana−Champaign, kindly provided the distances from the two current models of rHDL. Dr. Kirsten Arnvig McGuire deserves recognition for initiating mutagenesis studies in our laboratory and creating the original construct for the D9C mutant of proapoA-I.

REFERENCES

1. Gordon, D. J., Probsfield, J. L., Garrison, R. J., Neaton, J. D., Castelli, W. P., Knoke, J. D., Jacobs, D. R., Bangdiwala, D., and Tyroler, H. A. (1989) *Circulation 79*, 8−15.
2. Fielding, C. J., and Fielding, P. E. (1995) *J. Lipid Res. 36*, 211−228.
3. Xu, S., Laccotripe, M., Huang, X., Rigotti, A., Zannis, V. I., and Krieger, M. (1997) *J. Lipid Res. 38*, 1289−1298.
4. Wang, N., Silver, D. L., Costet, P., and Tall, A. R. (2000) *J. Biol. Chem. 275*, 33053−33058.
5. Rothblat, G. H., Mahlberg, F. H., Johnson, W. J., and Phillips, M. C. (1992) *J. Lipid Res. 33*, 1091−1097.
6. Jonas, A. (1991) *Biochim. Biophys. Acta 1084*, 205−220.
7. Rye, K.-A., and Barter, P. J. (1992) in *Structure and Function of Apolipoproteins* (Rosseneu, M., Ed.) pp 401−426, CRC Press, Boca Raton, FL.
8. Fidge, N. H. (1999) *J. Lipid Res. 40*, 187−201.
9. Segrest, J. P., Jones, M. K., DeLoof, H., Brouillette, C. G., Venkatachalapathi, Y. V., and Anantharamaiah, G. M. (1992) *J. Lipid Res. 33*, 141−166.
10. Palgunachari, M. N., Mishra, V. K., Lund-Katz, S., Phillips, M. C., Adeyeye, S. O., Alluri, S., Anantharamaiah, G. M., and Segrest, J. P. (1996) *Arterioscler. Thromb. Vasc. Biol. 16*, 328−338.
11. Marcel, Y. L., Provost, P. R., Koa, H., Raffai, E., Dac, N. V., Fruchart, J. C., and Rassart, E. (1991) *J. Biol. Chem. 266*, 3644−3653.
12. Minnich, A., Collet, X., Roghani, A., Cladaras, C., Hamilton, R. L., Fielding, C. J., and Zannis, V. I. (1992) *J. Biol. Chem. 267*, 16553−16560.
13. Sorci-Thomas, M. G., Thomas, M., Curtiss, L., and Landrum, M. (2000) *J. Biol. Chem. 275*, 12156−12163.
14. Cho, K.-Y., and Jonas, A. (2000) *J. Biol. Chem. 275*, 26821−26827.
15. Cho, K.-Y., Durbin, D. M., and Jonas, A. (2001) *J. Lipid Res. 42*, 379−389.
16. Luchoomun, J., Theret, N., Clavey, Y., Duchateau, P., Rosseneu, M., Brasseur, R., Denefle, P., Fruchart, J.-C., and Castro, G. R. (1994) *Biochim. Biophys. Acta 1212*, 319−326.
17. Brasseur, R., Lins, L., Vanloo, B., Ruysschaert, J. M., and Rosseneu, M. (1992) *Proteins: Struct., Funct., Genet. 13*, 246−257.
18. Phillips, J. C., Wriggers, W., Li, Z., Jonas, A., and Schulten, K. (1997) *Biophys. J. 73*, 2337−2346.
19. Segrest, J. P., Jones, M. K., Klon, A. E., Sheldahl, C. J., Hellinger, M., DeLoof, H., and Harvey, S. C. (1999) *J. Biol. Chem. 274*, 31755−31758.
20. Li, H.-H., Lyles, D. S., Thomas, M. J., Pan, W., and Sorci-Thomas, M. G. (2000) *J. Biol. Chem. 275*, 37048−37054.
21. McGuire, K. A., Davidson, W. S., and Jonas, A. (1996) *J. Lipid Res. 37*, 1519−1528.
22. Matz, C. E., and Jonas, A. (1982) *J. Biol. Chem. 257*, 4535−4540.
23. Jonas, A. (1986) *Methods Enzymol. 128*, 553−582.
24. Hefele-Wald, J., Krul, E. S., and Jonas, A. (1990) *J. Biol. Chem. 265*, 20037−20043.
25. Durbin, D. M., and Jonas, A. (1997) *J. Biol. Chem. 272*, 31333−31339.
26. Markwell, M. A., Haas, S. M., Bieber, L. L., and Tolbert, N. E. (1978) *Anal. Biochem. 87*, 206−210.
27. Chen, Y.-H., Yang, J. T., and Martinez, H. M. (1972) *Biochemistry 11*, 4120−4131.
28. Aune, K. C., and Tanford, C. (1969) *Biochemistry 8*, 4586−4590.
29. Sparks, D. L., Lund-Katz, S., and Phillips, M. C. (1992) *J. Biol. Chem. 267*, 25839−25847.
30. Lakowicz, J. R. (1986) in *Principles of Fluorescence Spectroscopy*, 3rd ed., pp 305−309, Plenum Press, New York and London.
31. Clegg, R. M. (1996) *Chem. Anal. (N.Y.) 137*, 179−194.
32. Weber, G. (1960) *Biochem. J. 75*, 335−352.
33. Hamman, B. D., Oleinikov, A. V., Jokhadze, G. G., Traut, R. R., and Jameson, D. M. (1996) *Biochemistry 35*, 16680−16686.
34. Gohlke, C., Murchie, A. I. H., Lilley, D. M. J., and Clegg, R. M. (1994) *Proc. Natl. Acad. Sci. U.S.A. 91*, 11660−11664.
35. Tricerri, M. A., Behling Agree, A. K., Sanchez, S. A., and Jonas, A. (2000) *Biochemistry 39*, 14682−14691.
36. Jonas, A. (1992) in *Structure and Function of Apolipoproteins* (Rosseneu, M., Ed.) pp 217−250, CRC Press, Boca Raton, FL.
37. Heithier, H., Fröhlich, M., Dees, C., Baumann, M., Häring, M., Gierschik, P., Schiltz, M., Vaz, W. L. C., Hekman, M., and Helmreich, E. J. M. (1992) *Eur. J. Biochem. 204*, 1169−1181.
38. Hamman, B. D., Oleinikov, A. V., Jokhadze, G. G., Bochkariov, D. E., Traut, R. R., and Jameson, D. M. (1996) *J. Biol. Chem. 271*, 7568−7573.
39. Haughland, R. P. (1996) *Handbook of Fluorescent Probes and Research Chemicals*, 6th ed., pp 29−30, Molecular Probes, Eugene, OR.
40. Rogers, D. P., Roberts, L. M., Lebowitz, J., Data, G., Anantharamaiah, G. M., Engler, J. A., and Brouillette, C. G. (1998) *Biochemistry 37*, 11714−11725.
41. Koppaka, V., Silvestro, L., Engler, J. A., Brouillette, C. G., and Axelsen, P. H. (1999) *J. Biol. Chem. 274*, 14541−14544.
42. Maiorano, J. N., and Davidson, W. S. (2000) *J. Biol. Chem. 275*, 17374−17380.
43. Davidson, W. S., Arnvig-McGuire, K., Kennedy, A., Kosman, J., Hazlett, T. L., and Jonas, A. (1999) *Biochemistry 38*, 14387−14395.
44. Jonas, A., Kézdy, K. E., and Hefele-Wald, J. (1989) *J. Biol. Chem. 264*, 4818−4824.
45. Jonas, A., Kézdy, K. E., Williams, M. I., and Rye, K.-A. (1988) *J. Lipid Res. 29*, 1349−1357.
46. Klon, A. E., Jones, M. K., Segrest, J. P., and Harvey, S. C. (2000) *Biophys. J. 79*, 1679−1685.

BI002815Q